Optics Communications 584 (2025) 131788

Contents lists available at ScienceDirect

Optics Communications

journal homepage: www.elsevier.com/locate/optcom

Generation and topological charge detection of multiple-vortex circular swallowtail tornado beams

Jiahao Guan, Zhenzhu Tong, Shaojie Xue, Hongling Yue, Xinyuan Qi *

School of Physics, Northwest University, Xi'an 710127, China

ARTICLE INFO

Keywords:
Optical vortices
Tornado waves
Topological charge
Phase modulation

ABSTRACT

Tornado waves are characterized by their unique ability to accelerate and twist light in radial and angular dimensions. These beams are generated by manipulating orbital angular momentum, but detecting their topological charge has been an uncharted territory. This paper presents a novel Tornado beam based on off-axis vortices-embedded circular swallowtail beams. We analyze the light propagation dynamics and employ cross-phase modulation to measure the topological charge of this circular swallowtail tornado beam with multiple vortices. Our method has been confirmed through computer simulations and experimental observations, proving its reliability. This technique offers a time-efficient and practical solution for measuring topological charges within tornado beams. This feature is highly beneficial for applications in light trapping and the advancement of optical communication systems.

1. Introduction

Wavefront shaping stands at the forefront of modern photonics, enabling the creation of structured light through various methods to generate customized light fields. This technology is a hot topic in research due to its extensive applications in imaging, nonlinear optics, and biophotonics [1–4]. Light structuring involves the spatial modulation of the light wave's phase, amplitude, and polarization, offering significant advantages over unstructured light. The Laguerre-Gauss mode [5] and the Bessel beam [6,7] are circularly symmetric solutions to the paraxial wave equation that carry optical vortices. These waves are characterized by the induction of topological charges into the wave field through the imprinting of a helical phase, resulting in an optical vortex that carries orbital angular momentum and exhibits a rotating phase structure as it propagates [8–11]. Caustics, another form of structured light, are points, lines, or surfaces where light rays converge, forming the envelope of a family of rays [12]. With fewer than four control parameters, there are seven fundamental caustic mutations, including folded, pointed, swallowtail, butterfly, elliptic umbilic, hyperbolic umbilic, and parabolic umbilic [13–15]. Airy beams, introduced in 2007 [16–18], Pearcey beams, observed in 2012 [19], and swallowtail and butterfly beams, systematically studied in 2017 [20,21] are notable for their auto-focusing and self-healing properties, which have been extensively studied [22–25]. Once the Airy beam carries with OAM, the vortex of modulated Airy beams follow the parabolic trajectory of the main blade [26]. In contrast, the vortices follow the power flow and, consequently, the trajectory of the main lobe when ring Airy beams and ring Airy Gaussian beams are modulated by an off-axis vortex or a pair of vortices [27–29]. Furthermore, combining ring Airy beams with power-exponent-phase may result in helical intensity distribution [30–32].

In 2020, a new type of wave packet, tornado waves (ToWs), was proposed by Brimis et al. through superposing two OAM ring Airy beams with opposite signs [33,34]. Subsequently, improved ToSWs composed of two circular swallowtails with opposite signs were proposed theoretically and experimentally [35,36]. Recently, Brimis et al. provided a new type of modified ToWs were proposed by injecting a limited number of off-axis optical vortices into a single toroidal Airy beam using wavefront shaping [37]. These ToWs have potential applications ranging from direct laser writing [38] to laser capture [39], nonlinear wave mixing [40], harmonic generation [41], and high-power terahertz generation [42].

Orbital angular momentum (OAM) states present new degrees of freedom for manipulating light [43,44]. To date, various techniques have been developed to measure the topological charges of vortex beams (VBs). Despite the optical setup for the interference method being straightforward, the experimental outcomes it provides often need to be more intuitive. Recently, researchers have employed phase modulation techniques to determine the topological charge (TC) of vortex beams, and the number of topological charges carried by the beam can be visually discerned by examining the intensity pattern of

* Corresponding author.
E-mail address: qixycn@nwu.edu.cn (X. Qi).

https://doi.org/10.1016/j.optcom.2025.131788
Received 18 February 2025; Received in revised form 18 March 2025; Accepted 20 March 2025
Available online 1 April 2025

the diffraction pattern after phase modulation. The modulation phases commonly employed in these methods include twisted (cross phase, CP) [45], lens phase [46], and sinusoidal phase [47]. Recently, interest in embedding multiple vortex singularities within the main beam, rather than just a single vortex, has increased, driven by the need to enhance communication capabilities and manipulate multiple particles. However, until now, there have been no reports on detecting multi-vortex topological charges in tornado beams that are accelerated and distorted in both radial and angular directions.

In this study, we introduce a novel type of tornado-like intensity profile by implanting a select number of off-axis optical vortices into a single circular swallowtail beams (CSBs). Employing a combination of theoretical and experimental methodologies, we have successfully observed the light propagation behavior and measured the topological charge of multiple-vortex circular swallowtail tornado beams (MVCSTBs), utilizing the cross-phase (CP) measurement technique. Our findings present a time-efficient and practical method for quantifying the topological charges of multiple vortices within a rapidly autofocusing beam. This capability holds significant potential for light manipulation and optical communication systems applications.

2. Theory

In the field of optics, according to catastrophe theory, the caustic field $C_n(a)$ is expressed by a standard diffraction catastrophe integral as:

$$C_n(a) = \int_R \exp[ip_n(a,s)]ds. \tag{1}$$

The properties of the caustic field are determined by the regular potential function $p_n(a,s)$, which is defined as

$$p_n(a,s) = s^n + \sum_{j=1}^{n-2} a_j s^j, \tag{2}$$

where $a = (a_1, a_2, \ldots, a_j)$ is a set of dimensionless control parameters a_j, and $a = 1, 2, \ldots, n-2$; s is a state parameter. For the case of $n = 5$, the fifth-order catastrophe field $C_5(a_1, a_2, a_3)$ — also named as swallowtail beam $Sw(a_1, a_2, a_3)$ can be expressed as:

$$Sw(a_1,a_2,a_3) = \int_{-\infty}^{\infty} \exp[\mathrm{i}(s^5 + a_3 s^3 + a_2 s^2 + a_1 s)]ds. \tag{3}$$

In this section, we propose a new type of tornado wave. By incorporating a finite number of optical vortices with the phase of Φ_v into a single circular swallowtail light field ψ_{CS}, we obtain the light field of multiple-vortex circular swallowtail tornado beams (MVCSTBs) described as follows:

$$\psi_{\mathrm{MVCSTBs}}(r,\theta,0) = A_0 \psi_{\mathrm{CS}} \exp(\mathrm{i}\Phi_v), \tag{4}$$

where A_0 is the constant amplitude of the electric field, $\psi_{\mathrm{CS}} = Sw\left(\frac{r_0 - r}{aw}, 0, 0\right)\exp\left[-b\frac{(r_0-r)^2}{w^2}\right]$ is the light field of the circular swallowtail beams, r_0 is the primary ring radius [25], a is spatial distribution factors that affect the beam intensity distribution, and b is a constant. w is the initial widths of the beams. $\Phi_v = \sum_{j=1}^{M} l_j\theta_j$ is the phases of introduced vortices, M is the number of vortices, l_j is the topological charge of each vortex, and θ_j represents the azimuth of each centrifugal optical vortex, defined as:

$$\theta_j = \arctan\left(\frac{x - x_j}{y - y_j}\right), \tag{5}$$

where x_j and y_j are coordinates representing the center of the vortex.

In paraxial optical systems, the propagation of such a beam is governed by the paraxial wave equation [25]:

$$2ik\frac{\partial\psi}{\partial z} + \frac{\partial^2\psi}{\partial r^2} + \frac{1}{r}\frac{\partial\psi}{\partial r} + \frac{1}{r^2}\frac{\partial^2\psi}{\partial\theta^2} = 0, \tag{6}$$

where $k = 2\pi/\lambda$ stands for the wave number and λ is the laser wavelength.

By inserting three vortices ($l_1 = l_2 = l_3 = -2$) in a circular swallowtail beam, MVCSTBs is achieved as shown in Fig. 1. The distance between the beam center and the vortex center is $r_p = 0.7$ mm.

3. Experiment and simulation

In this paper, we will experimentally verify the generation of MVCSTBs and measure their topological charges via cross-phase modulation. The experimental device is the same as that in Ref. [48]. The Gaussian beam with wavelength $\lambda = 532$ nm is extended and collimated from the solid-state laser through a beam expander composed of two lenses ($f_1 = 50$ mm, $f_2 = 250$ mm), and the beam matches the polarization requirements of the spatial light modulator (SLM) after passing through the polarizer P. The beam is then incident on a spatial light modulator [SLM, pixel size 8.2 μm, pixel resolution (H) 1920 × (V) 1200 pixels] via a beam-splitter (BS), on which a pre-designed hologram loaded can be generated by interference between MVCSTBs and the plane wave. The beam modulated by the SLM passes through the BS and then through a 4f system consisting of two lenses ($f_3 = 100$ mm, $f_4 = 100$ mm) and a filter (F). The filter F is used to select the first diffraction order of the beam. By adjusting the position of the charge-coupled device (CCD), the expected light intensity distribution of MVCSTBs at different transmission distances can be obtained.

Although there is no analytical solution for MVCSTBs in free space, we have employed the angular spectrum theory [49] to simulate the propagation of light beams numerically. In the simulation, we set $A_0 = 1$, $\lambda = 532$ nm, $r_0 = 0.8$ mm, $a = 0.06$, $w = 0.5$ mm, $b = 0.5$. Unless otherwise stated, these parameters remain unchanged.

First, we considered the simple scenario where the circular swallowtail beams are modulated by two vortex phases, each with a topological charge of $l_j = 2$ ($j = 1, 2$) and symmetrically positioned relative to the beam's center. Specifically, the vortices are located at $(x_1, y_1) = (-0.7, 0)$ and $(x_2, y_2) = (0.7, 0)$. The propagation dynamics of this initial configuration are illustrated in Fig. 2. Fig. 2(a) presents a side view of the MVCSTBs' propagation. The propagation dynamics of this beam are very similar to the recently introduced ToWs [33,34]. Moreover, compared with introducing a limited number of vortices into a single annular airy beam [37], the swallowtail diffraction mutations have higher dimensions, more diversity, and tunability. Figs. 2(b1)–2(b5) display the transverse intensity distribution maps at various distances z, as indicated by the white dashed lines in Fig. 2(a), while Figs. 2(c1)–2(c5) show the corresponding phase distributions. From Fig. 2(a), it is observable that the beam follows a parabolic trajectory. At the same time, the two vortex singularities in the initial plane of the MVCSTBs develop into four vortex singularities, each with a topological charge of 1, indicated by the black circles in Figs. 2(c1) and (c5). This evolution can be attributed to the instability of higher-order vortex singularities [37]. Incorporating off-axis vortices leads to the synchronous counterclockwise rotation of high-intensity lobes during beam propagation, resulting in an intensity profile reminiscent of a tornado. The high-intensity lobes in ToWs trace a spiral path with a decreasing radius and pitch [33,34]. Additionally, the cross-sectional images in Figs. 2(b1)–2(b5) reveal that the rotation of the high-intensity lobe is, to some extent, associated with the rotation of the optical vortex. When the two vortices are in proximity, the size of each high-intensity lobe diminishes as the beam propagates [37]. Our experiments further validated that embedding a finite number of off-axis vortices within a single circular swallowtail beam induces the beam to rotate freely and display a tornado-like intensity pattern. By comparing the experimental cross-sectional intensity distributions in Figs. 2(d1)–2(d5) with the numerical simulation results in Figs. 2(b1)–2(b5), a high degree of agreement between the experimental and simulated results is apparent.

The mathematical expression of the cross phase in Cartesian coordinates is:

$$\Phi_C(x,y) = u(x^m\cos\phi - y^n\sin\phi)(x^m\sin\phi + y^n\cos\phi), \tag{7}$$

therefore, the MVCSTBs optical field with cross-phase modulation can be expressed as:

$$\psi_C(r,\theta,0) = \psi_{\mathrm{MVCSTBs}}(r,\theta,0)\exp(\mathrm{i}\Phi_C), \tag{8}$$

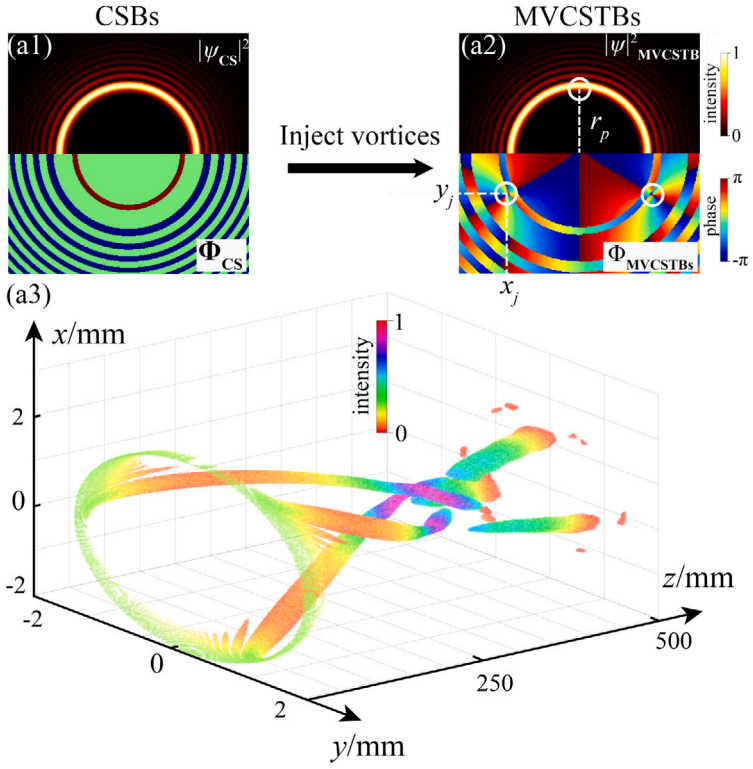

Fig. 1. Formation of MVCSTBs.

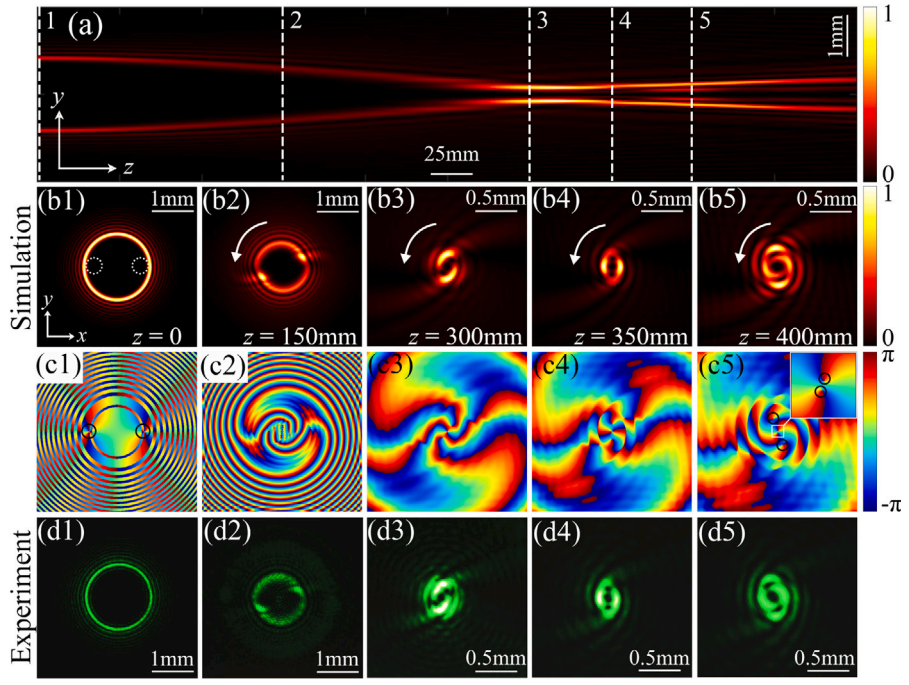

Fig. 2. Propagation of the MVCSTBs in the free space with $l_1 = l_2 = 2$. (a) Dissemination side view of MVCSTBs; (b1–b5) corresponding to (a) the $x - y$ cross-section intensity distribution of the white dotted line; (c1–c5) phase distribution corresponds to (b1–b5) respectively; (d1–d5) Experimental results correspond to (b1–b5) respectively.

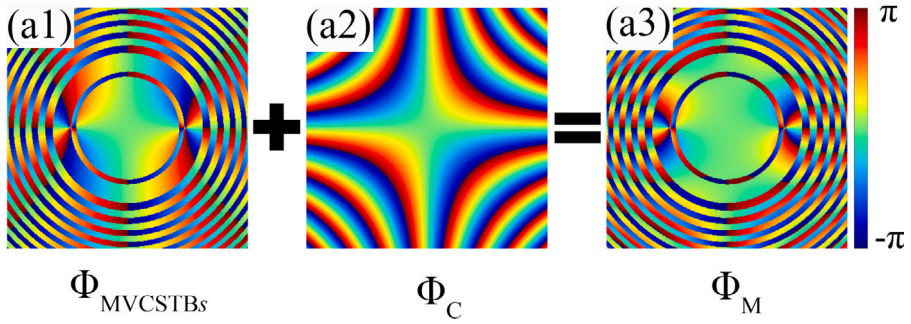

Fig. 3. Phase construction of CP-modulated MVCSTBs.

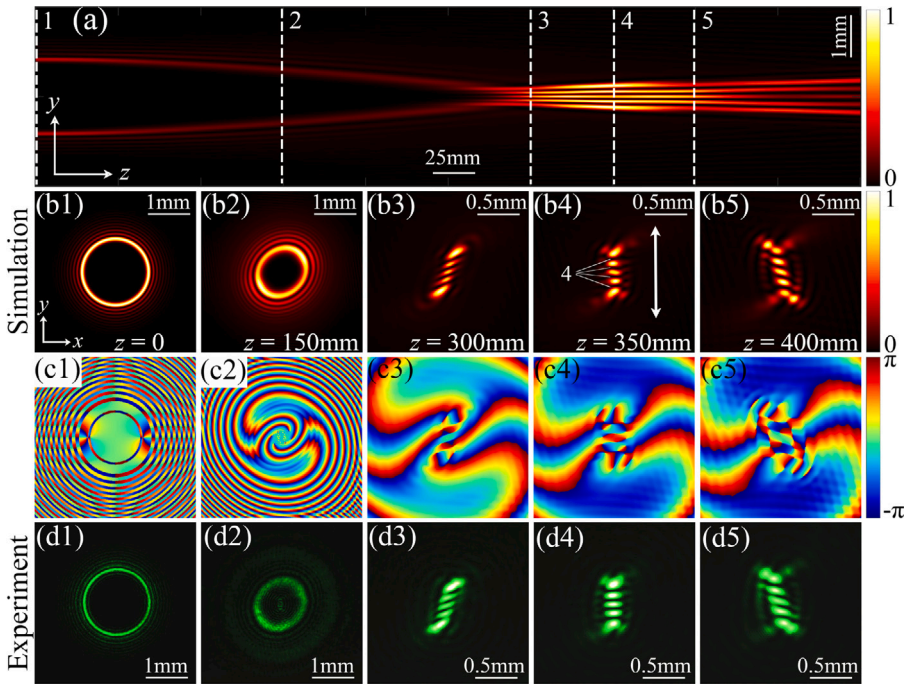

Fig. 4. Propagation of the CP-modulated MVCSTBs in the free space. (a) Side view of the propagation of the MVCSTBs modulated by CP; (b1)–(b5) Simulated transverse intensity distributions at different z in (a) marked with white dotted lines; (c1)–(c5) Phase distributions corresponds to (b1)–(b5), respectively; (d1–d5) Experimental observations corresponding to (b1)–(b5), respectively.

where the parameter u is the conversion rate, the azimuth factor ϕ is the rotation angle of the conversion beam on a specific plane, and n and m are positive integers. When $\phi = 0$, $n = 1$, $m = 1$, the formula can be simplified to: $\Phi_C(r,\theta) = ur^2 \cos\theta \sin\theta$ in cylindrical coordinate system. Similar to the literature [45,50,51], here we only consider this low-order case to study the measurement of topological charges.

The physical mechanism by which CP measures the topological charge of a single vortex singularity is believed to be effective anisotropic diffraction, resulting in the rapid splitting of the vortex singularity [51]. Meanwhile, the anisotropic diffraction effect of CP can also be used for topological charge measurement of multi-vortex singularities [52]. Figs. 3(a1)–3(a3), respectively, represent the phase of MVCSTBs, the cross-phase, and the phase of MVCSTBs after being modulated by the cross phase. We set $u = 5$, $\phi = 0$, $n = 1$, $m = 1$.

Therefore, we use CP to modulate MVCSTBs in the initial plane and study its propagation characteristics, as shown in Fig. 4. The beam parameters here are the same as those in Fig. 2. The side view of the propagation of CP-modulated MVCSTBs is displayed in Fig. 4(a). Figs. 4(b1)–4(b5) and Figs. 4(c1)–4(c5) show the transverse intensity and phase distributions corresponding to different distances z, which correspond to the white dashed lines in Fig. 4(a) respectively. Compared with Fig. 2, it can be found that there is a significant change in the light intensity distribution after autofocus. Due to the mode conversion characteristic caused by CP, the hidden topological charge information in MVCSTBs is presented in the form of a set of separated nodes, where the number of gaps between nodes (the "dark region" between high-energy regions) is equal to the sum of the number of topological charges in MVCSTBs. The arrangement of "dark regions" is vertical. Therefore, the CP modulation method can still be used to measure topological charges of multiple vortex singularities. At the same time, we also conducted experimental verification, as shown in Figs. 4(d1)–4(d5), and it can be seen that the experimental results are consistent with the simulation results.

Next, we consider cases with negative topological charges, where $M = 3$ and $l_1 = l_2 = l_3 = -2$. In the case of more embedded singularities, for convenience, all embedded singularities are symmetrically distributed on a circle with radius $r_p = 0.7$ mm, and the three vortices are placed in the position shown by the white dotted line in Fig. 5(a1). Figs. 5(a1–a5) and 5(c1–c5) show the intensity and phase distributions of MVCSTBs and MVCSTBs with CP on the $z = 0$, 250 mm, 300 mm, 350 mm, 400 mm plane (illustration), and the experimental results are shown in Fig. 5(b1–b5) and 5(d1–d5), respectively. Due to the addition of off-axis vortices ($l_1 = l_2 = l_3 = -2$), the beam's high-intensity lobes rotate clockwise during propagation, as shown in Figs.

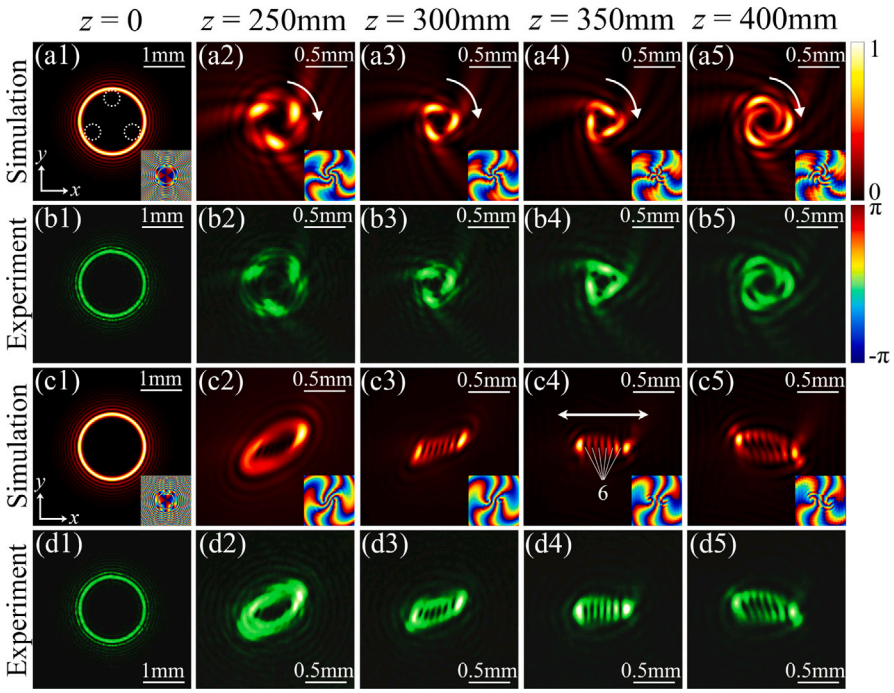

Fig. 5. Detected of MVCSTBs with negative topological charges, $l_1 = l_2 = l_3 = -2$, by using the cross-phase method. (a1–a5) Simulated transverse intensity distribution at different z. (b1–b5) Experimental observations corresponding to (a1–a5); (c1–c5) Simulated transverse intensity distribution with CP-modulated; (d1–d5) Experimental observations corresponding to (c1–c5). Three white dotted circles indicate the positions of three vortices, and the insets at the right-bottom indicate their phase distributions.

5(a1)–5(a5) is precisely the opposite of the case in Figs. 2(b1)–2(b5), where the embedding topological charges is positive. Similarly, we observe that as the beam propagates, the size of each high-intensity lobe also decreases as it propagates and then diffuses. For MVCSTBs with CP in this case, the hidden topological charges information in MVCSTBs is also presented as a set of separated nodes, where the number of gaps between nodes (the "dark region" between the high energy regions) is equal to the sum of the number of topological charges in MVCSTBs, due to the mode switching properties caused by CP. However, it is worth noting that the arrangement of the "dark zone" at this time is horizontal, which differs from the case in Figs. 4(b1)–4(b5), where the embedded topological charges are positive. Therefore, we can judge the positive and negative topological charges in MVCSTBs by the arrangement and number of "dark regions". By comparing the measured section intensity distribution in Figs. 5(b1–b5) and 5(d1–d5), it can be found that the experimental results are highly consistent with the numerical simulation results shown in Figs. 5(a1–a5) and 5(c1–c5).

In the following, we investigate where multiple vortex points are placed symmetrically. We superimpose multiple topologically charged vortices placed symmetrically in the center of the beam to form a regular polygon. Similar to the previous discussion, all vortices have the exact topological charges (l_j= +2). Figs. 6(a1–a5) and 6(b1–b5) depict the intensity distribution and phase distribution of each beam in the initial plane (z = 0). The positions of the vortices are covered by polygons, with circles (white dashed lines) at each vertex marking the position of each vortex. The intensity distribution and experimental results corresponding to MVCSTBs in the focal area (z = 340 mm) are shown in Figs. 6(c1–c5) and 6(d1–d5). The presence of optical vortices leads to the azimuth modulation of the beam intensity and the formation of uniformly distributed high-intensity lobes. In all symmetric configurations, the vortex's rotation follows the strength lobe's rotation [37]. The intensity distribution and experimental results corresponding to MVCSTBs with CP in the focal area (z = 340 mm) are shown in Figs. 6(e1–e5) and 6(f1–f5). With the increment of vortex numbers, the intensity distribution will change somewhat. The intensity of the central region will decrease, and the gap numbers between nodes are 4, 6, 8, 10, and 12, respectively, corresponding to the different cases of the number of vortex singularities (M = 2 ~ 6). Here, the gaps between nodes in each subgraph equal the number of topological charges carried by MVCSTBs. The simulation results are in good agreement with the experimental results.

At the same time, we also study situations where the vortex is asymmetrical and the topological charges are not equal. In Fig. 7, we give four examples of this asymmetric configuration. More specifically, as we see in Figs. 7(a1)–7(a4), in Fig. 7(a1), we consider the case of a single vortex (l = 4). In Fig. 7(a2), two vortices ($l_1 = l_2 = 3$) are located at an azimuth that is not perpendicular to each other. In Fig. 7(a3), the two vortices ($l_1 = -4$, $l_2 = -2$) are at azimuth angles perpendicular to each other. In Fig. 7(a4), the three vortices ($l_1 = -4$, $l_2 = -1$, $l_3 = -3$) are located at different azimuths and radial positions. Figs. 7(c1–c4) and 7(d1–d4) show the intensity distribution and experimental results corresponding to the focal region (z = 340 mm) of MVCSTBs with CP in the case where the vortex configuration is asymmetric and the topological charges are not equal. The simulation results are consistent with the experimental results, and the number of gaps between nodes still equals the total number of topological charges carried by all vortex points.

Finally, although the total OAM of a beam in free space is a conserved quantity, we expect it to be conserved for all possible geometric configurations and topological charges. For example, when vortices have topological charges with opposite signs on the initial plane z = 0, as they propagate, they will approach the center of the beam and annihilate in pairs of l = +1 and l = −1, see Ref. [27]. As a result, the vortices will annihilate in pairs without intensity modulation and vortices [37]. However, we investigated the case where vortex positive and negative topological charges are present simultaneously and are not equal. Figs. 8(a1)–8(a5) shows five different scenarios in which six vortex singularities are embedded in the circle (at the position of the dotted white line), and the specific topological charges are marked inside the dotted white line. Figs. 8(b1)–8(b5) corresponds to its phase mode respectively. Figs. 8(c1–c5) and 8(d1–d5) correspond to the numerical simulation and experimental results when the propagation distance z = 340 mm in five cases. The experimental measurement results agree well with the simulation results. The number of gaps

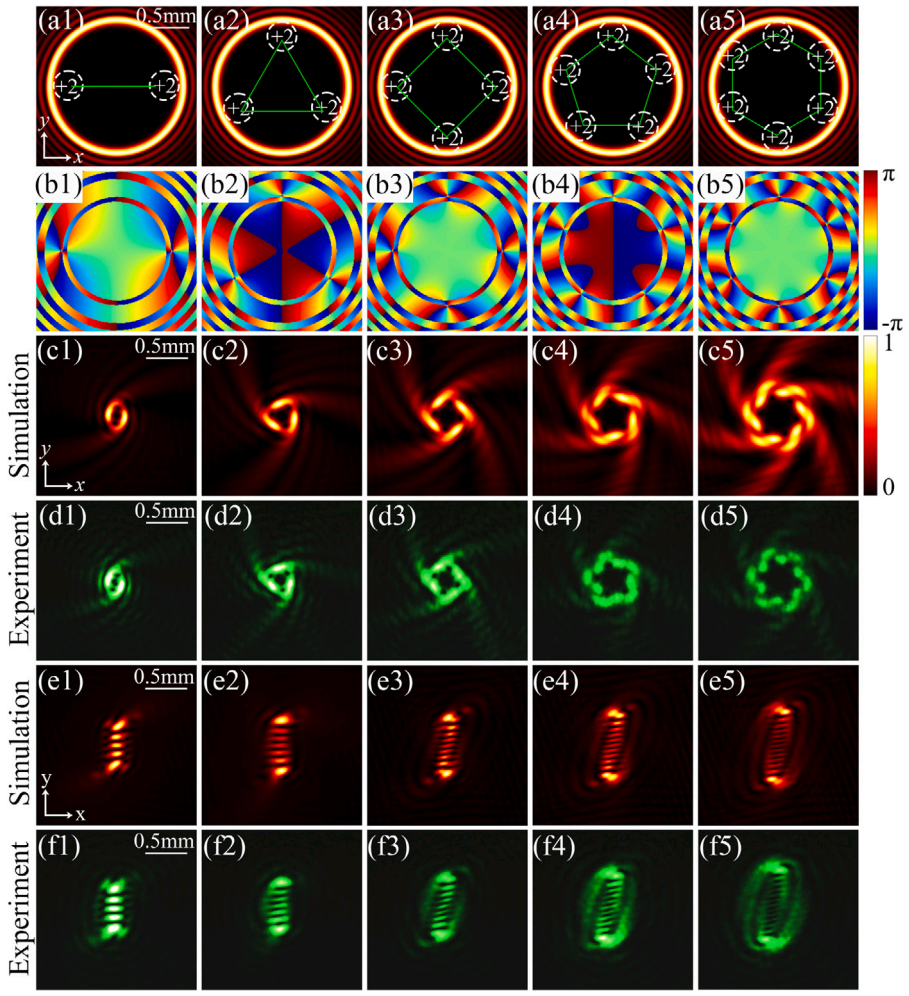

Fig. 6. Topological charges detection of symmetrically configured vortices. (a1–a5) The initial intensity distribution at the initial plane $z = 0$ (The dotted white circles mark the position and size of each vortex); (b1–b5) phase distribution corresponds to (a1–a5) respectively; (c1–c5) correspond to the intensity distribution of MVCSTBs on the $z = 340$ mm plane, respectively. (d1–d5) experimental results corresponding to (c1–c5); (e1–e5) corresponding to the intensity distribution of MVCSTBs with CP on the $z = 340$ mm plane, respectively; (f1–f5) experimental results correspond to (e1–e5).

between nodes equals the net topological charge carried by the embedded vortex singularities. Here, the number of gaps between nodes in each case is 5, 6, 8, −6, and −7, corresponding to the total number of singular topological charges in different cases. The feasibility of this measurement method in detecting MVCSTBs topological charges is further proved.

4. Conclusion

In conclusion, we have developed a wavefront shaping technique by integrating a limited number of off-axis optical vortices into a single circular swallowtail beam, thereby generating optical tornadoes. By applying both simulation and experimental approaches, we observed the propagation dynamics of light and, for the first time, measured the topological charges of these tornado beams. We discovered that a tornado beam forms when the net charges of the vortices are non-zero, and as the number of vortices increases, so does the number of main lobes in the tornado light. Our results also confirmed that the rotation and twist of the tornado beams become more pronounced with increasing propagation distance. The experiment further demonstrated that the number of diffraction fringe dark traces, or nodal lines, in CP-modulated tornado beams, corresponds to the net topological charges of the tornado light. The insights from our work have expanded our understanding of tornado light and hold promise for applications in light capture and optical communication systems.

CRediT authorship contribution statement

Jiahao Guan: Writing – original draft, Visualization, Validation, Software, Project administration, Investigation, Data curation, Conceptualization. **Zhenzhu Tong:** Investigation, Formal analysis. **Shaojie Xue:** Investigation, Formal analysis. **Hongling Yue:** Investigation, Formal analysis. **Xinyuan Qi:** Writing – review & editing, Supervision, Project administration, Formal analysis, Conceptualization.

Declaration of competing interest

The authors declare that they have no known competing financial interests or personal relationships that could have appeared to influence the work reported in this paper.

Acknowledgments

This work was supported by the National Natural Science Foundation of China (NSFC) (N0. 12174307), and the authors thank Prof. Peilong Hong for the constructive discussion with this work.

Data availability

Data will be made available on request.

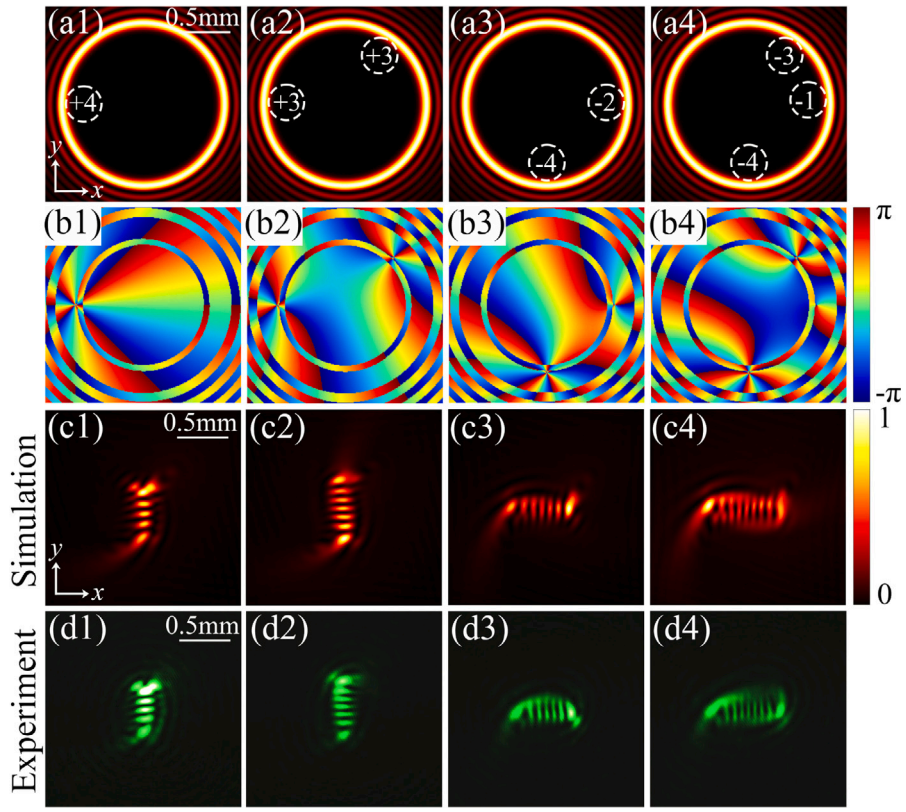

Fig. 7. Topological charges detection of asymmetrically configured vortices. (a1–a5) The initial intensity distribution at the initial plane $z = 0$ (The dotted white circles mark the position and size of each vortex); (b1–b5) phase distribution corresponds to (a1–a5) respectively; (c1–c5) corresponds to the intensity distribution of MVCSTBs with CP on the $z = 340$ mm plane, respectively. (d1–d5) Experimental results correspond to (c1–c5).

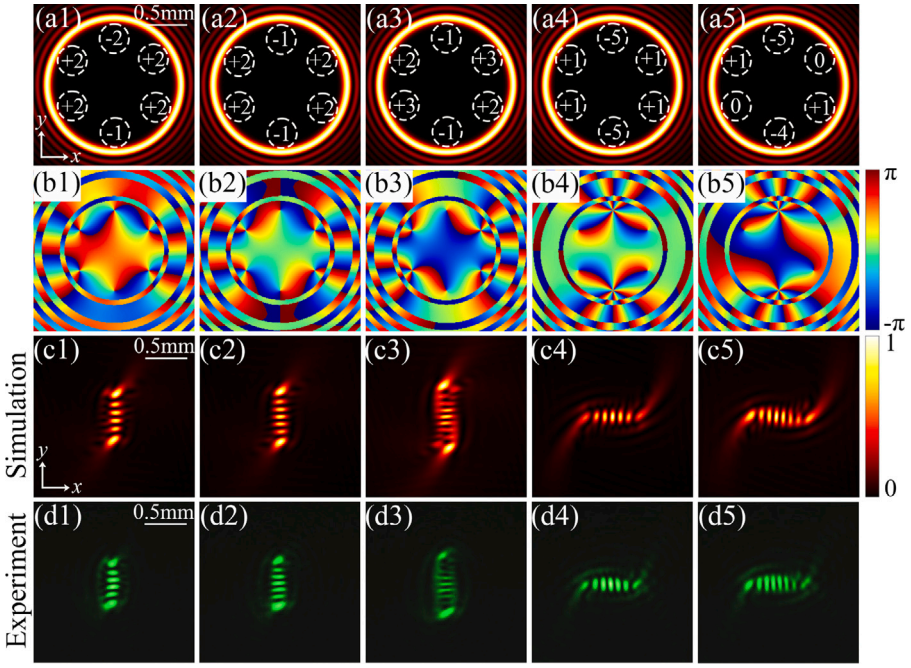

Fig. 8. The situation where both positive and negative topological charges are present simultaneously. (a1–a5) The initial intensity distribution at the initial plane $z = 0$ (the dotted white line marks the position and size of each vortex); The phase distribution (b1–b5) corresponds to (a1–a5) respectively; (c1–c5) corresponds to the intensity distribution of MVCSTBs with CP modulation on the $z = 340$ mm plane, respectively. (d1–d5) Experimental results correspond to (c1–c5).

References

[1] Halina Rubinsztein-Dunlop, Andrew Forbes, M.V. Berry, M.R. Dennis, David L. Andrews, Masud Mansuripur, Cornelia Denz, Christina Alpmann, Peter Banzer, Thomas Bauer, Ebrahim Karimi, Lorenzo Marrucci, Miles Padgett, Monika Ritsch-Marte, Natalia M. Litchinitser, Nicholas P. Bigelow, C. Rosales-Guzmán, A. Belmonte, J.P. Torres, Tyler W. Neely, Mark Baker, Reuven Gordon, Alexander B. Stilgoe, Jacquiline Romero, Andrew G. White, Robert Fickler, Alan E. Willner,

Guodong Xie, Benjamin McMorran, Andrew M. Weiner, Roadmap on structured light, J. Opt. (ISSN: 2040-8986) 19 (1) (2016) 013001, http://dx.doi.org/10.1088/2040-8978/19/1/013001.

[2] L. Allen, V.E. Lembessis, M. Babiker, Spin-orbit coupling in free-space Laguerre–Gaussian light beams, Phys. Rev. A (ISSN: 1094-1622) 53 (5) (1996) R2937–R2939, http://dx.doi.org/10.1103/physreva.53.r2937.

[3] Zhongxi Wang, N. Zhang, X.-C. Yuan, High-volume optical vortex multiplexing and de-multiplexing for free-space optical communication, Opt. Express (ISSN: 1094-4087) 19 (2) (2011) 482, http://dx.doi.org/10.1364/oe.19.000482.

[4] S.H. Tao, X.-C. Yuan, J. Lin, X. Peng, H.B. Niu, Fractional optical vortex beam induced rotation of particles, Opt. Express (ISSN: 1094-4087) 13 (20) (2005) 7726, http://dx.doi.org/10.1364/opex.13.007726.

[5] L. Allen, M.W. Beijersbergen, R.J.C. Spreeuw, J.P. Woerdman, Orbital angular momentum of light and the transformation of laguerre-Gaussian laser modes, Phys. Rev. A (ISSN: 1094-1622) 45 (11) (1992) 8185–8189, http://dx.doi.org/10.1103/physreva.45.8185.

[6] J. Durnin, Exact solutions for nondiffracting beams I the scalar theory, J. Opt. Soc. Amer. A (ISSN: 1520-8532) 4 (4) (1987) 651, http://dx.doi.org/10.1364/josaa.4.000651.

[7] D. McGloin, K. Dholakia, Bessel beams: Diffraction in a new light, Contemp. Phys. (ISSN: 1366-5812) 46 (1) (2005) 15–28, http://dx.doi.org/10.1080/0010751042000275259.

[8] D. Gauthier, P. Rebernik Ribič, G. Adhikary, A. Camper, C. Chappuis, R. Cucini, L.F. DiMauro, G. Dovillaire, F. Frassetto, R. Géneaux, P. Miotti, L. Poletto, B. Ressel, C. Spezzani, M. Stupar, T. Ruchon, G. De Ninno, Tunable orbital angular momentum in high-harmonic generation, Nat. Commun. (ISSN: 2041-1723) 8 (1) (2017) http://dx.doi.org/10.1038/ncomms14971.

[9] Alison M. Yao, Miles J. Padgett, Orbital angular momentum: origins, behavior and applications, Adv. Opt. Photonics (ISSN: 1943-8206) 3 (2) (2011) 161, http://dx.doi.org/10.1364/aop.3.000161.

[10] Zhenxing Liu, Yuanyuan Liu, Yougang Ke, Yachao Liu, Weixing Shu, Hailu Luo, Shuangchun Wen, Generation of arbitrary vector vortex beams on hybrid-order Poincaré sphere, Photonics Res. (ISSN: 2327-9125) 5 (1) (2016) 15, http://dx.doi.org/10.1364/prj.5.000015.

[11] Yuanhui Wen, Ioannis Chremmos, Yujie Chen, Jiangbo Zhu, Yanfeng Zhang, Siyuan Yu, Spiral transformation for high-resolution and efficient sorting of optical vortex modes, Phys. Rev. Lett. (ISSN: 1079-7114) 120 (19) (2018) http://dx.doi.org/10.1103/physrevlett.120.193904.

[12] Yu. A. Kravtsov, Yu. I. Orlov, Caustics, catastrophes and wave fields, in: Springer Series on Wave Phenomena, Springer Berlin Heidelberg, (ISSN: 0931-7252) ISBN: 9783642598876, 1993, http://dx.doi.org/10.1007/978-3-642-59887-6.

[13] H. Trinkaus, F. Drepper, On the analysis of diffraction catastrophes, J. Phys. A: Math. Gen. (ISSN: 1361-6447) 10 (1) (1977) L11–L16, http://dx.doi.org/10.1088/0305-4470/10/1/003.

[14] M.V. Berry, C. Upstill, IV catastrophe optics: Morphologies of caustics and their diffraction patterns, in: Progress in Optics, Elsevier, (ISSN: 0079-6638) ISBN: 9780444854452, 1980, pp. 257–346, http://dx.doi.org/10.1016/s0079-6638(08)70215-4.

[15] Ernesto Espíndola-Ramos, Gilberto Silva-Ortigoza, Citlalli Teresa Sosa-Sánchez, Israel Julián-Macías, Omar de Jesús Cabrera-Rosas, Paula Ortega-Vidals, Adriana González-Juárez, Ramón Silva-Ortigoza, Mercedes Paulina Velázquez-Quesada, G.F. Torres del Castillo, Paraxial optical fields whose intensity pattern skeletons are stable caustics, J. Opt. Soc. Amer. A (ISSN: 1520-8532) 36 (11) (2019) 1820, http://dx.doi.org/10.1364/josaa.36.001820.

[16] M.V. Berry, N.L. Balazs, Nonspreading wave packets, Am. J. Phys. 36 (3) (1979) 264–267, http://dx.doi.org/10.1119/1.11772.

[17] Georgios A. Siviloglou, Demetrios N. Christodoulides, Accelerating finite energy airy beams, Opt. Lett. (ISSN: 1539-4794) 32 (8) (2007) 979, http://dx.doi.org/10.1364/ol.32.000979.

[18] G.A. Siviloglou, J. Broky, A. Dogariu, D.N. Christodoulides, Observation of accelerating airy beams, Phys. Rev. Lett. (ISSN: 1079-7114) 99 (21) (2007) http://dx.doi.org/10.1103/physrevlett.99.213901.

[19] James D. Ring, Jari Lindberg, Areti Mourka, Michael Mazilu, Kishan Dholakia, Mark R. Dennis, Auto-focusing and self-healing of pearcey beams, Opt. Express 20 (17) (2012) 18955–18966, http://dx.doi.org/10.1364/OE.20.018955.

[20] Alessandro Zannotti, Falko Diebel, Martin Boguslawski, Cornelia Denz, Optical catastrophes of the swallowtail and butterfly beams, New J. Phys. (ISSN: 1367-2630) 19 (5) (2017) 053004, http://dx.doi.org/10.1088/1367-2630/aa6ecd.

[21] Alessandro Zannotti, Falko Diebel, Cornelia Denz, Dynamics of the optical swallowtail catastrophe, Optica (ISSN: 2334-2536) 4 (10) (2017) 1157, http://dx.doi.org/10.1364/optica.4.001157.

[22] John Broky, Georgios A. Siviloglou, Aristide Dogariu, Demetrios N. Christodoulides, Self-healing properties of optical airy beams, Opt. Express 16 (17) (2008) 12880–12891, http://dx.doi.org/10.1364/OE.16.012880.

[23] Xingyu Chen, Dongmei Deng, Jingli Zhuang, Xi Peng, Dongdong Li, Liping Zhang, Fang Zhao, Xiangbo Yang, Hongzhan Liu, Guanghui Wang, Focusing properties of circle pearcey beams, Opt. Lett. (ISSN: 1539-4794) 43 (15) (2018) 3626, http://dx.doi.org/10.1364/ol.43.003626.

[24] Pablo Vaveliuk, Óscar Martínez-Matos, Yu-Xuan Ren, Rong-De Lu, Dual behavior of caustic optical beams facing obstacles, Phys. Rev. A (ISSN: 2469-9934) 95 (6) (2017) http://dx.doi.org/10.1103/physreva.95.063838.

[25] Houan Teng, Yixian Qian, Yanping Lan, Yiming Cai, Abruptly autofocusing circular swallowtail beams, Opt. Lett. (ISSN: 1539-4794) 46 (2) (2021) 270, http://dx.doi.org/10.1364/ol.415709.

[26] Masato Suzuki, Keisaku Yamane, Takashige Omatsu, Ryuji Morita, Propagation-invariant vortex Airy beam whose singular point follows its main lobe, New J. Phys. (ISSN: 1367-2630) 23 (11) (2021) 113043, http://dx.doi.org/10.1088/1367-2630/ac37af.

[27] Yunfeng Jiang, Kaikai Huang, Xuanhui Lu, Propagation dynamics of abruptly autofocusing Airy beams with optical vortices, Opt. Express (ISSN: 1094-4087) 20 (17) (2012) 18579, http://dx.doi.org/10.1364/oe.20.018579.

[28] Bo Chen, Chidao Chen, Xi Peng, Yulian Peng, Meiling Zhou, Dongmei Deng, Propagation of sharply autofocused ring Airy Gaussian vortex beams, Opt. Express (ISSN: 1094-4087) 23 (15) (2015) 19288, http://dx.doi.org/10.1364/oe.23.019288.

[29] Xiang Zhang, Peng Li, Sheng Liu, Bingyan Wei, Shuxia Qi, Xinhao Fan, Shouheng Wang, Yuan Zhang, Jianlin Zhao, Autofocusing of ring Airy beams embedded with off-axial vortex singularities, Opt. Express (ISSN: 1094-4087) 28 (6) (2020) 7953, http://dx.doi.org/10.1364/oe.387961.

[30] Peng Li, Sheng Liu, Tao Peng, Gaofeng Xie, Xuetao Gan, Jianlin Zhao, Spiral autofocusing Airy beams carrying power-exponent-phase vortices, Opt. Express (ISSN: 1094-4087) 22 (7) (2014) 7598, http://dx.doi.org/10.1364/oe.22.007598.

[31] Sang-Hyuk Lee, Yohai Roichman, David G. Grier, Optical solenoid beams, Opt. Express (ISSN: 1094-4087) 18 (7) (2010) 6988, http://dx.doi.org/10.1364/oe.18.006988.

[32] Barak Hadad, Sahar Froim, Harel Nagar, Tamir Admon, Yaniv Eliezer, Yael Roichman, Alon Bahabad, Particle trapping and conveying using an optical Archimedes' screw, Optica (ISSN: 2334-2536) 5 (5) (2018) 551, http://dx.doi.org/10.1364/optica.5.000551.

[33] Apostolos Brimis, Konstantinos G. Makris, Dimitris G. Papazoglou, Tornado waves, Opt. Lett. (ISSN: 1539-4794) 45 (2) (2020) 280, http://dx.doi.org/10.1364/ol.45.000280.

[34] Dimitris Mansour, Apostolos Brimis, Konstantinos G. Makris, Dimitris G. Papazoglou, Spiraling light: Generating optical tornados, Phys. Rev. A (ISSN: 2469-9934) 105 (5) (2022) http://dx.doi.org/10.1103/physreva.105.053514.

[35] Junjie Jiang, Danlin Xu, Zhenwu Mo, Xuezhen Cai, Haoyu Huang, Yong Zhang, Haobin Yang, Haiqi Huang, You Wu, Lingling Shui, Dongmei Deng, Generation and control of tornado waves by means of ring swallowtail vortex beams, Opt. Express (ISSN: 1094-4087) 30 (7) (2022) 11331, http://dx.doi.org/10.1364/oe.453165.

[36] Yong Zhang, JiaLong Tu, ShangLing He, YiPing Ding, ZhiLi Lu, You Wu, GuangHui Wang, XiangBo Yang, DongMei Deng, Experimental generation of the polycyclic tornado circular swallowtail beam with self-healing and auto-focusing, Opt. Express (ISSN: 1094-4087) 30 (2) (2022) 1829, http://dx.doi.org/10.1364/oe.446818.

[37] Apostolos Brimis, Konstantinos G. Makris, Dimitris G. Papazoglou, Optical vortices shape optical tornados, Opt. Express (ISSN: 1094-4087) 31 (17) (2023) 27582, http://dx.doi.org/10.1364/oe.495836.

[38] Christian R. Ocier, Corey A. Richards, Daniel A. Bacon-Brown, Qing Ding, Raman Kumar, Tanner J. Garcia, Jorik van de Groep, Jung-Hwan Song, Austin J. Cyphersmith, Andrew Rhode, Andrea N. Perry, Alexander J. Littlefield, Jinlong Zhu, Dajie Xie, Haibo Gao, Jonah F. Messinger, Mark L. Brongersma, Kimani C. Toussaint, Lynford L. Goddard, Paul V. Braun, Direct laser writing of volumetric gradient index lenses and waveguides, Light: Sci. Appl. (ISSN: 2047-7538) 9 (1) (2020) http://dx.doi.org/10.1038/s41377-020-00431-3.

[39] Junjie Jiang, Danlin Xu, Zhenwu Mo, Xuezhen Cai, Haoyu Huang, Yong Zhang, Haobin Yang, Haiqi Huang, You Wu, Lingling Shui, Dongmei Deng, Generation and control of tornado waves by means of ring swallowtail vortex beams, Opt. Express (ISSN: 1094-4087) 30 (7) (2022) 11331, http://dx.doi.org/10.1364/oe.453165.

[40] Vincent Boyer, Alberto M. Marino, Raphael C. Pooser, Paul D. Lett, Entangled images from four-wave mixing, Science (ISSN: 1095-9203) 321 (5888) (2008) 544–547, http://dx.doi.org/10.1126/science.1158275.

[41] Desheng Ding, Jian-yu Lu, Second-harmonic generation of thenth-order bessel beam, Phys. Rev. E (ISSN: 1095-3787) 61 (2) (2000) 2038–2041, http://dx.doi.org/10.1103/physreve.61.2038.

[42] Rusnė Ivaškevičiūtė-Povilauskienė, Paulius Kizevičius, Ernestas Nacius, Domas Jokubauskis, Kęstutis Ikamas, Alvydas Lisauskas, Natalia Alexeeva, Ieva Matulaitienė, Vytautas Jukna, Sergej Orlov, Linas Minkevičius, Gintaras Valušis, Terahertz structured light: nonparaxial airy imaging using silicon diffractive optics, Light: Sci. Appl. (ISSN: 2047-7538) 11 (1) (2022) http://dx.doi.org/10.1038/s41377-022-01007-z.

[43] Zhaoyang Zhang, Feng Li, G. Malpuech, Yiqi Zhang, O. Bleu, S. Koniakhin, Changbiao Li, Yanpeng Zhang, Min Xiao, D.D. Solnyshkov, Particlelike behavior of topological defects in linear wave packets in photonic graphene, Phys. Rev. Lett. (ISSN: 1079-7114) 122 (23) (2019) http://dx.doi.org/10.1103/physrevlett.122.233905.

[44] Feng Li, Sergei V. Koniakhin, Anton V. Nalitov, Evgeniia Cherotchenko, Dmitry D. Solnyshkov, Guillaume Malpuech, Min Xiao, Yanpeng Zhang, Zhaoyang Zhang, Simultaneous creation of multiple vortex-antivortex pairs in momentum space in photonic lattices, Adv. Photonics (ISSN: 2577-5421) 5 (06) (2023) http://dx.doi.org/10.1117/1.ap.5.6.066007.

[45] Donghui Shen, Daomu Zhao, Measuring the topological charge of optical vortices with a twisting phase, Opt. Lett. (ISSN: 1539-4794) 44 (9) (2019) 2334, http://dx.doi.org/10.1364/ol.44.002334.

[46] Xuejuan Liu, Meidi Wang, Lei Guo, Shubo Cheng, Shaohua Tao, Measuring the photonic topological charge of power-exponent-phase vortex beam via cross phase, Appl. Phys. Lett. (ISSN: 1077-3118) 123 (3) (2023) http://dx.doi.org/10.1063/5.0157586.

[47] Xuejuan Liu, Lei Guo, Meidi Wang, Shuo Liu, Shubo Cheng, Shaohua Tao, Wenxing Yang, Measuring the topological charge of a helico-conical vortex beam via the lens phase, Appl. Phys. Lett. (ISSN: 1077-3118) 123 (17) (2023) http://dx.doi.org/10.1063/5.0170906.

[48] Zhixi Wen, Xin Wan, Yundong He, Yuandan Wang, ZengRun Wen, Yuanmei Gao, Wenjing Zhang, Xinyuan Qi, Light localization in defective periodic photonic moiré-like lattices, J. Opt. Soc. Amer. A (ISSN: 1520-8532) 39 (12) (2022) 2291, http://dx.doi.org/10.1364/josaa.473693.

[49] Ting-Chung Poon, Taegeun Kim, Engineering Optics with MATLAB®, World Scientific, ISBN: 9789812773135, 2006, http://dx.doi.org/10.1142/6166.

[50] Haosen Pu, Osami Sasaki, Takamasa Suzuki, Samuel Choi, Measurements of phase distributions of optical vortices based on the sinusoidal phase modulation method, Opt. Contin. (ISSN: 2770-0208) 1 (11) (2022) 2287, http://dx.doi.org/10.1364/optcon.473876.

[51] Yuan Li, Guo Liang, Xubo Hu, Controllable splitting and bidirectional rotating of optical vortices due to cross phase, J. Modern Opt. (ISSN: 1362-3044) 69 (13) (2022) 734–740, http://dx.doi.org/10.1080/09500340.2022.2086714.

[52] Jian Yu, Huihong Long, Shandong Tong, Yuan Luo, Peichao Zheng, Zhe Zhang, Zhiyong Bai, Topological charges measurement of circular Bessel Gaussian beam with multiple vortex singularities via cross phase, Opt. Express (ISSN: 1094-4087) 32 (9) (2024) 15460, http://dx.doi.org/10.1364/oe.523000.